AAAS–Newcomb Cleveland Prize
To Be Awarded for an Article or a Report Published in *Science*

The AAAS-Newcomb Cleveland Prize is awarded annually to the author of an outstanding paper published in *Science* from August through July. This competition year starts with the 4 August 1978 issue of *Science* and ends with that of 27 July 1979. The value of the prize is $5000; the winner also receives a bronze medal.

Reports and Articles that include original research data, theories, or synthesis and are fundamental contributions to basic knowledge or technical achievements of far-reaching consequence are eligible for consideration for the prize. The paper must be a first-time publication of the author's own work. Reference to pertinent earlier work by the author may be included to give perspective.

Throughout the year, readers are invited to nominate papers appearing in the Reports or Articles sections. Nominations must be typed, and the following information provided: the title of the paper, issue in which it was published, author's name, and a brief statement of justification for nomination. Nominations should be submitted to AAAS-Newcomb Cleveland Prize, AAAS, 1515 Massachusetts Avenue, NW, Washington, D.C. 20005. Final selection will rest with a panel of distinguished scientists appointed by the Board of Directors.

The award will be presented at a session of the annual meeting. In case of multiple authorship, the prize will be divided equally between or among the authors.

Reports

Barrier Island Configuration

Abstract. *The 11 Virginia barrier islands are undergoing rapid changes in shoreline configuration. If this trend continues for another 100 years, two capelike features will develop. The process responsible for this island-chain pattern may be a standing edge wave trapped between Assateague Island and Cape Charles.*

In an earlier report (*1*) we concluded that the shoreline configuration along Assateague Island is related to mesoscale processes within the inshore zone and that these processes must be consistent along the mid-Atlantic coast. We have now expanded our research to include the 11 Virginia barrier islands immediately south of Assateague Island (Fig. 1). Results show that these islands are behaving as a chain and are undergoing rapid and systematic changes that are leading to the accentuation of an overall crescentic or arcuate configuration. If the past trends continue, two capelike features may develop within the next century.

We measured changes in the shoreline configuration (erosion-deposition-orientation) of the 11 Virginia barrier islands in maps and charts dating from 1852 to 1974 (*2*). Using an orthogonal coordinate system with a grid spacing of 500-m intervals, we recorded shoreline intersections with the across-the-shore grid transects. This was repeated ten times for the shoreline data (maps) available. By this method we assembled a 10 by 135 temporal-spatial data matrix of shoreline positions.

The correlation between the rate of shoreline change and shoreline orientation along Assateague Island was +0.93 (*1*). Similar analysis for the Virginia islands (Fig. 1) yielded correlations from +0.94 to −0.94. Both the magnitude and the sign of the correlation are dependent on the overall orientation of the island (Fig. 2A).

High positive correlations between shoreline change and orientation were found for islands with an orientation less than 28° east of north and large negative correlations for islands oriented greater than 28° east of north. In general, the high islandwide rates of erosion occurred with island orientations near 28° east of north, and as such these most rapidly eroding shorelines are nearly perpendicular to the direction of the highest waves (north-northeast to northeast) from passing storms. Apparently even small departures in shoreline orientation from 28° east of north result in large changes in the relationship between erosion rates and orientation (Fig. 2A). None of the Virginia islands is oriented at exactly 28° east of north.

With differential rates of shoreline change along the islands, the net effect is that the islands tend to rotate either clockwise or counterclockwise. To quantify this rotation, we calculated the ratio of the rate of shoreline change for the north end to the south end of each island (E_n/E_s). Using these data and the relationships shown in Fig. 2, A and B, we generalized two models for barrier island dynamics. In the first, the Wallops Island model (Fig. 2C), the island rotation is clockwise ($E_n/E_s < 1$), so that the island orientation, θ, tends to increase with time; however, as θ increases, the rate of shoreline change decreases (negative correlation), and thus $d\theta/dt$ decreases. This negative feedback drives the system toward an equilibrium configuration.

In the second model, the Cedar Island model (Fig. 2D), the island rotation is

Length Limit for Reports: The average length of individual Reports in *Science* has been steadily increasing. At the same time, the number of pages allotted to Reports has remained constant and cannot be increased. The net result has been that fewer Reports on fewer subjects are being published; many that receive excellent reviews must be rejected for lack of space. The overall rejection rate is more than 80 percent. In order to increase the acceptance rate we will enforce the length requirements: one to seven double-spaced manuscript pages of text, including the references and note, and two displayed items which together will occupy no more than half of a published page. Long Reports are subject to delays in reviewing and editorial consideration. After Reports are reviewed, those that exceed the length limit will be returned to authors for shortening before a final decision is made. Reports that are short will not be subject to these delays.

Statistical Review of Papers: As part of our continuing effort to improve the quality of papers published in *Science*, Reports and Articles that depend on statistical inference for their conclusions will be sent to statisticians (in addition to other referees) for review.

0036-8075/79/0427-0401$00.50/0

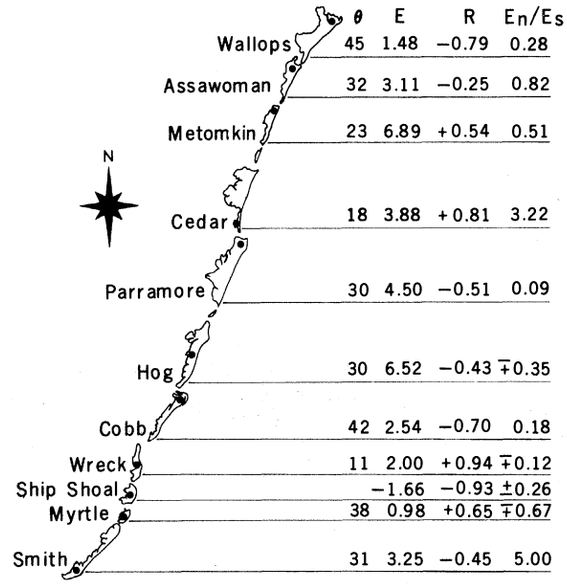

Fig. 1. Location map and data summary for the 11 Virginia barrier islands: θ is the mean island orientation in degrees east of north; E is the mean rate of change of the shoreline (in meters per year); R is the correlation between the shoreline change rate and the orientation; and E_n/E_s is the ratio of the shoreline change rate for the north end to the south end of the island. The circles on each island designate the location of the center of island rotation. Plus and minus signs on E_n/E_s indicate accretion (−) and erosion (+), respectively. Where no sign is specified, erosion (+) has occurred at both ends of the islands.

counterclockwise ($E_n/E_s > 1$) and θ becomes smaller. For Cedar Island, θ is 18° east of north and the rates of shoreline change are large (positive correlation). As θ declines, the rates of shoreline change decrease and the process of rotation slows. As in the case of the earlier model, this model results in an equilibrium configuration.

The orientation and position of each of the islands relative to the others were assessed in terms of the islandwide rates of change and the relative direction and magnitudes of rotation. The silhouettes of the barrier island chain (Fig. 3) compare the current configuration with that predicted if the past trends continue through the next century. In order for the resulting configuration to be realized, the overall shapes of the individual islands will, of course, undergo major changes.

Figure 3 suggests the growth of two capelike features; thus the climatological integration of erosional variations with orientation described here is, in effect, a model for the evolution of sedimentary capes. Initiation of this process could be associated with (i) irregularities in the orientation of the coast due to regional-scale geology or (ii) variations in the intensity of processes occurring along the coast. Inman and his co-workers recently reported on the possibility of standing edge waves being responsible for large-scale shoreline and shelf features (*3*). We examined the distribution of edge wave nodes and antinodes for a hypothetical trapped standing wave between the shoals of Fisherman's Point (on the southern end of Assateague Island) and the shoals near Cape Charles. An edge wave modal number 3 would result in antinodes at almost the exact location of each of the two capelike features suggested in Fig. 3. Fisherman's Point and the related shoals have been growing rapidly to the south for more than 150 years (*4*), and so considerable readjustment to a shorter edge wave may have occurred. This does not mean that only edge wave modal number 3 is involved, or that edge waves are responsible for the large sedimentary capes of the Atlantic coast. However, our studies of shoreline dynamics for the 122 km of coast between Cape Hatteras and Cape Lookout indicate that edge waves may play an important role in regional scale variations in shoreline dynamics (*5*).

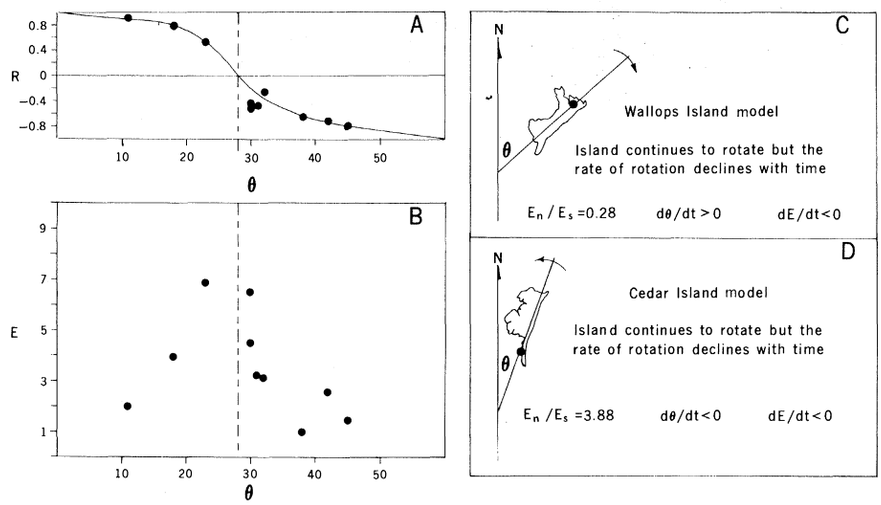

Fig. 2 (above). (A) Within-island correlations of the mean rate of shoreline change and shoreline orientation. (B) Mean rates of shoreline change (E) (in meters per year) versus the average orientation (θ) of the islands. (C) A model of the dynamics for rotating islands in which erosion is negatively correlated with orientation. (D) A model of the dynamics for rotating islands in which erosion is positively correlated with orientation. The data for Ship Shoal are not included because this island is nearly round. Fig. 3 (left). The predicted configuration of the Virginia barrier island chain, assuming that past trends in shoreline change continue for the next century.

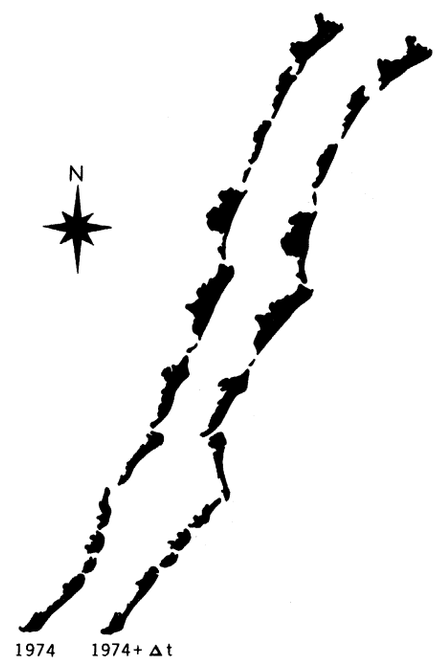

ROBERT DOLAN
BRUCE HAYDEN
CONRAD JONES
Department of Environmental Sciences, University of Virginia, Charlottesville 22903

References and Notes

1. R. Dolan, B. Hayden, J. Heywood, L. Vincent, *Science* **197**, 49 (1977).
2. T. E. Rice, W. Niedoroda, A. P. Pratt, in *The Virginia Coast Reserve Study 1976* (The Nature Conservancy, Arlington, Va., 1976), pp. 117–279.
3. R. T. Guza and D. L. Inman, *J. Geophys. Res.* **80**, 2997 (1975); D. L. Inman, C. E. Nordstrom, R. E. Flick, *Annu. Rev. Fluid Mech.* **8**, 275 (1976).
4. C. E. Gawne, thesis, University of Illinois (1966).
5. R. Dolan, B. Hayden, W. Felder, *J. Geol.*, in press.

6. This research was supported by the Office of Naval Research, Geography Programs, the National Aeronautics and Space Administration, the National Park Service, and earlier work sponsored by the Geography Programs Office, U.S. Geological Survey.

5 June 1978, revised 17 October 1978

Flow Cytometry: A High-Resolution Instrument for Everyone

Abstract. *A new flow configuration for flow cytometry has been devised in which a flat, laminar stream of water, containing the stained cells in a narrow central sector, is formed on a microscope cover slip by a pressurized jet of water directed onto the glass at low angle. The stream of cells is viewed by means of a fluorescence microscope with incident illumination and a pulse photometer. Coupled to a multichannel pulse height analyzer, the instrument constitutes a stable and easy-to-operate flow cytometer with a resolution equal to or better than a coefficient of variance of 1.4 percent in measurements of cellular DNA.*

Quantitative measurements of the cellular content of various cell constituents by flow cytometry is becoming widely used for both research and diagnostic purposes (*1*). The principle of the method is to pass a narrow stream of cells, stained with a fluorescent dye which binds quantitatively to the constituent under study, through a beam of exciting light and to measure the intensity of the resulting pulses of fluorescence. The distribution of cells with regard to such a constituent—for example, DNA—can thus be determined with high precision and at a rate of about 10^3 cells per second. Advanced flow cytometers, which measure several cell parameters simultaneously, are now commercially available. However, there is a growing need for a simple and inexpensive instrument for routine tasks.

One approach to the construction of such an instrument is to utilize a fluorescence microscope (*2*), which provides high aperture optics for both the excitation and the fluorescence light. We describe here a new flow configuration which, when implemented on a standard fluorescence microscope with a suitable photometer, constitutes a relatively inexpensive and easy-to-operate flow cytometer with high resolution and stability.

Our idea is to create a laminar flow on a microscope cover slip by means of a jet of water directed onto the glass at low angle (Fig. 1A). In this configuration, the cells are centered in the jet by hydrodynamic focusing (*3*) and are thereby confined to a narrow and stable section of the flow on the cover slip, which is viewed by an inverted fluorescence microscope in incident light—that is, with the excitation light focused through the detection objective.

The nozzle (Specialty Glass Products part 91216) producing the pressurized jet of water, 80 μm in diameter, is similar to that used in flow cytometers where the exciting light intersects the water jet in air (*4*). The water is drained from the cover slip by suction through a hypodermic needle. The microscope (Leitz Diavert) has a ×40/1.30 oil immersion objective. It is fitted with an incident light illuminator (Ploemopak) and a superpressure mercury lamp (Osram HBO 100) with stabilized power supply (*5*). The nozzle is mounted on the object guide of the microscope stage. When viewed through the microscope binocular, the water jet can thus be readily positioned to obtain the configuration shown in Fig. 1B. A photomultiplier tube (PMT) (EMI 9659QB) is mounted on the phototube of the binocular. A variable slit in the phototube limits the area viewed by the PMT. The pulse length of the PMT is about 5 μsec; thus sample flow rates of the order of 10^3 cells per second can be used. The PMT pulses are fed to a multichannel pulse height analyzer.

The pulse height distribution obtained for rat thymocytes, stained for DNA measurement with a combination of ethidium bromide and mithramycin (*6*), exhibits a symmetrical peak with a full width at half maximum corresponding to a coefficient of variance (CV)—that is, relative standard deviation—of 1.4 percent. A typical plot is shown in Fig. 2. For these cells we routinely obtain CV $\leqq$ 1.5 percent, with no need of readjustments between samples. Since the true CV for these cells is not known, it is not clear to what extent the mesured width reflects the resolution of the instrument. Hence, we conclude that its resolution is equal to or better than 1.4 percent.

The performance of our instrument does not seem to be critically dependent on the exact physical characteristics of the flow system, such as the position and angle of the water jet or its driving pressure (*7*). Hence, optimum conditions are easily achieved and stability appears excellent. The instrument's characteristics are described in detail elsewhere (*8*).

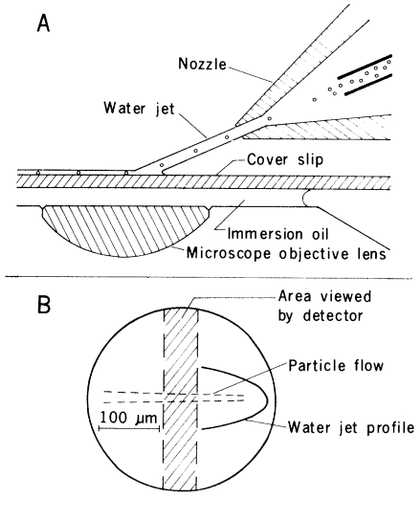

Fig. 1. The essential part of the flow system. (A) A collimated beam of cells in a pressurized water jet, formed by hydrodynamic focusing, hits a glass cover slip at low angle to form a flat, laminar stream with the cells confined to a narrow sector. The cover slip is viewed by means of an inverted fluorescence microscope with incident illumination. (B) The flow as it appears in the microscope. The shaded area indicates the section viewed by the fluorescence detector.

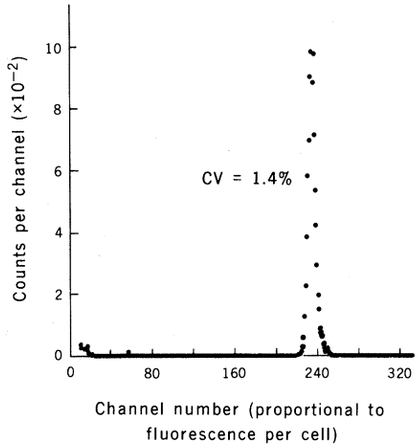

Fig. 2. A plot of the fluorescence (DNA) per cell as obtained for rat thymocytes stained with ethidium bromide and mithramycin, which bind quantitatively to DNA. The full width of the peak at half maximum corresponds to a coefficient of variance (CV) of 1.4 percent. The peak, representing 10,600 cells, was registered in 29 seconds. A small peak, due to cell doublets, was observed at twice the channel number of the present peak.

0036-8075/79/0427-0403$00.50/0